Self-Assembling Cannabinomimetics: Supramolecular Structures of *N*-Alkyl Amides

Stefan Raduner,[†] William Bisson,[‡] Ruben Abagyan,[‡] Karl-Heinz Altmann,[†] and Jürg Gertsch*,[†]

Department of Chemistry and Applied Biosciences, ETH Zurich, Wolfgang-Pauli-Strasse 10, CH-8093 Zürich, Switzerland, and Molecular Biology, The Scripps Research Institute, TSRI, 10550 North Torrey Pines Road, TPC-28, La Jolla, California 92037

Certain fatty acid *N*-alkyl amides from the medicinal plant *Echinacea* activate cannabinoid type-2 (CB$_2$) receptors. In this study we show that the CB$_2$-binding *Echinacea* constituents dodeca-2*E*,4*E*-dienoic acid isobutylamide (**1**) and dodeca-2*E*,4*E*,8*Z*,10*Z*-tetraenoic acid isobutylamide (**2**) form micelles in aqueous medium. In contrast, micelle formation is not observed for undeca-2*E*-ene-8,10-diynoic acid isobutylamide (**3**), which does not bind to CB$_2$, or structurally related endogenous cannabinoids, such as arachidonoyl ethanolamine (anandamide). The critical micelle concentration (CMC) range of **1** and **2** was determined by fluorescence spectroscopy as 200−300 and 7400−10000 nM, respectively. The size of premicelle aggregates, micelles, and supermicelles was studied by dynamic light scattering. Microscopy images show that compound **1**, but not **2**, forms globular and rod-like supermicelles with radii of approximately 75 nm. The self-assembling *N*-alkyl amides partition between themselves and the CB$_2$ receptor, and aggregation of *N*-alkyl amides thus determines their *in vitro* pharmacological effects. Molecular mechanics by Monte Carlo simulations of the aggregation process support the experimental data, suggesting that both **1** and **2** can readily aggregate into premicelles, but only **1** spontaneously assembles into larger aggregates. These findings have important implications for biological studies with this class of compounds.

Purple coneflower (*Echinacea purpurea* and *E. angustifolia*) preparations are widely used herbal medicines for the treatment of the common cold and upper respiratory infections,[1,2] with an estimated sales volume in 2002 of $500 million in the U.S. alone.[3] Fatty acid *N*-alkyl amides (alkylamides) are a class of bioavailable lipophilic compounds, which are generally found in *Echinacea* species. There is increasing evidence that *N*-isobutyl amides inhibit acute inflammation and might contribute to the beneficial effects reported for *Echinacea*.[4−6] We have recently shown that two major alkylamides from *Echinacea*, dodeca-2*E*,4*E*-dienoic acid isobutylamide (**1**) and dodeca-2*E*,4*E*,8*Z*,10*Z*-tetraenoic acid isobutylamide (**2**) (Figure 1), constitute a new class of cannabinomimetics.[4] Compounds **1** and **2** bind to and activate the peripheral cannabinoid receptor (CB$_2$) more strongly than the endogenous cannabinoids arachidonoyl ethanolamine (anandamide; AA) and 2-arachidonoyl-glycerol (2-AG) (Figure 1); **1** also has moderate affinity for the CB$_1$ receptor. Activation of CB$_2$ receptors has been associated with distinct immunomodulatory effects, such as inhibition of tumor necrosis factor alpha (TNF-α) expression.[7]

During radioligand experiments with compounds **1** and **2** a biphasic displacement of the radioligand [³H]-CP55,940 was observed, which raised the question whether *N*-alkyl amide CB$_2$ binding is competing with *N*-alkyl amide self-aggregation as a function of concentration.[4] In order to determine whether aggregation could be responsible for discontinuous CB$_2$ receptor binding of **1** and **2**, the aim of the current study was to examine the aggregation behavior of *N*-isobutyl amides **1**, **2**, and **3** (the latter has no affinity to cannabinoid receptors) and the structurally related endogenous cannabinoids anandamide and 2-AG in aqueous medium. Aggregation of amphiphilic molecules can result in the formation of three types of supramolecular structures: premicelles, which are generally clusters of less than 10 monomers; micelles, which are aggregates of amphiphilic molecules as colloidal dispersion capable of entrapping lipophilic molecules (e.g., fluorescent dyes); and higher order complexes of micelles (supermicelles). Since *N*-alkyl amides are likely to contribute to the pharmacological action of *Echinacea* preparations, it is important to understand aggregation and micellization of these compounds, in particular because such
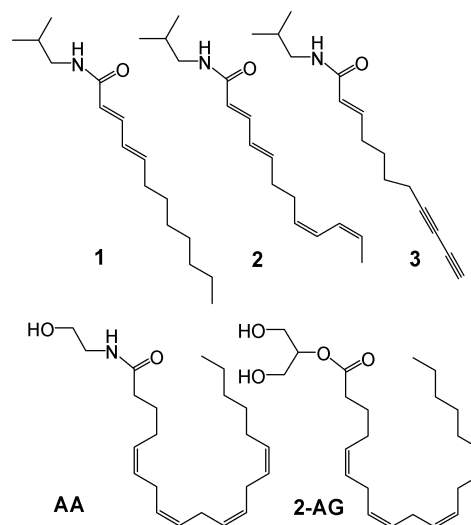
Figure 1. Structures of *N*-alkyl amides from *Echinacea purpurea* (**1**−**3**) and endogenous cannabinoids arachidonoyl ethanolamine (AA) and 2-arachidonoylglycerol (2-AG).

processes are known to influence the pharmacokinetic and pharmacodynamic behavior of drugs.[8]

Results and Discussion

Aqueous solutions of **1** and **2** were found to display a pronounced Tyndall effect (Rayleigh scattering) at concentrations of >2 μM. At concentrations of <3 μM the colloidal particles formed by **1** and **2** could not be filtered out with 0.2 μm cellulose acetate filters nor did they settle upon standing at room temperature. In contrast, neither compound **3**, which is structurally related to **1** and **2** but does not bind to CB$_2$, nor arachidonoyl ethanolamine (anandamide) or 2-arachidonoylglycerol (2-AG) (Figure 1) showed a Tyndall effect. Higher concentrations of **1** (>3 μM) resulted in the formation of floating precipitates when stored at room temperature over 24−72 h. In the dispersed state, the particles were separate and moved erratically with Brownian motion, whereas the flocked state was characterized by particles, which clumped together in aggregates under the influence of van der Waals forces.[9] In order to study

* Corresponding author. E-mail: juerg.gertsch@pharma.ethz.ch.
† ETH Zurich.
‡ Scripps Research Institute.
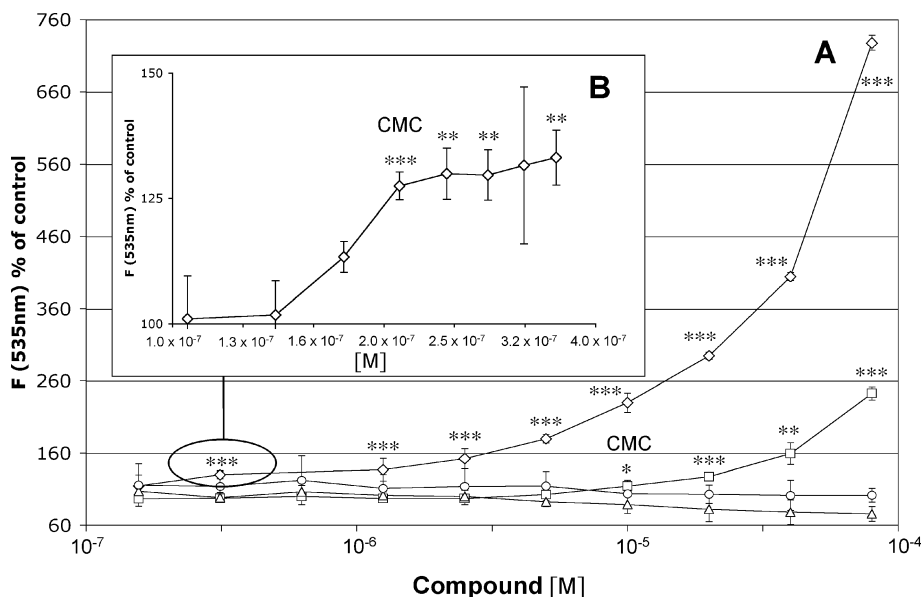
Figure 2. Dye micellization to determine CMC values of **1** and **2**. (A) Incorporation of fluorescein (micellization) by **1** (diamonds) and **2** (squares). 2-AG (circles) and AA (triangles) do not lead to dye micellization. (B) Micellization at low concentrations of **1**. $*p = \leq 0.05$; $**p = \leq 0.01$; $***p = \leq 0.001$.

whether the flocculation of **1** was due to formation of supermicelles and aggregates thereof, we attempted to characterize the aggregation process of the *N*-alkyl amides.

In this study the critical micelle concentrations (CMCs) of **1** and **2** were determined by fluorescent dye micellization employing a modification of the method reported by Eliyahu et al.[10] Fluorescence techniques have proved to be powerful tools for studying the microstructure of colloidal systems. The CMC was calculated as the concentration at which a significant first increase in fluorescence could be detected (Figure 2), due to internalization of fluorescein into micelles. The CMC ranges measured in deionized water (pH < 7.0) at 30 °C were 200−300 nM (pmol/L) for **1** and 7400−10000 nM (pmol/L) for **2**, respectively (Figure 2). In receptor binding buffer, which contained 0.5 mg/mL bovine serum albumin (BSA), the CMC ranges were not significantly different, thus indicating that the micellization of compounds **1** and **2** is not markedly influenced by the presence of BSA.

In order to study the monomer to premicelle transition and the subsequent formation of micelles and supermicelles, photon correlation spectroscopy (PCS) measurements were performed (see Experimental Section). The CONTIN distribution algorithm[11] was used to characterize changes in the size of the colloidal particles formed by **1** and **2** in both filtered receptor binding buffer and deionized water free of external particles. The data presented in Figure 3 show that compounds **1** and **2** spontaneously assembled into premicellar and micellar aggregates with sizes below 100 nm. It was not possible to distinguish between premicelles and micelles of **2** in the CONTIN distribution. Moreover, increasing concentrations of **2** did not result in increasing particle sizes (Figure 3), indicating that no further aggregation beyond micelles occurs. This was also confirmed by microscopic analysis, where **2** did not show structures detectable with an immersion oil phase contrast objective. On the other hand, increasing concentrations of **1** resulted in increasing particle size (Figure 3), suggesting continuous assembly of premicelles into micelles and/or supermicelles. Particle size distribution measurements of 200 nM **1** (the CMC) yielded an average particle diameter of approximately 76 nm (Figure 4).

Suspensions (50 µM) of **1** were analyzed microscopically. Images from oil immersion phase contrast microscopy showed that compound **1** assembles into supermicelles with both globular and rod-like shapes (Figure 5). The radii of the rod-like and globular supermicelles were determined as approximately 75 nm, which is
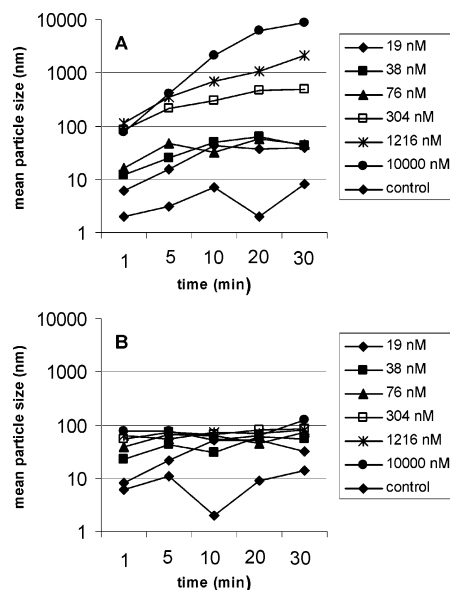

Figure 3. Particle formation over time of compounds **1** and **2** measured by dynamic light scattering. (A) Compound **1** forms premicellar aggregates at concentrations as low as 38 nM, and increasing concentrations lead to increasing mean particle sizes. (B) Increasing concentrations of compound **2** do not lead to increasing mean particle sizes. Mean values of two independent experiments.

around twice the radius of a micelle (Figure 4). Rod-like supermicelles have been proposed as anisotropic structures of colloids that show a strong first-order transition from the fluid phase of small micelles to a liquid crystalline phase of large supermicelles.[12]

To determine the effect of the aggregation of **1** on the interaction with the CB$_2$ receptor, quantitative radioligand assays were carried out with increasing concentrations of the compound. In order to quantify receptor binding, we measured the displacement of the cannabinoid radioligand [³H]CP55,940 from the human CB$_2$ receptor expressed in HEK cells as published previously.[4] In Figure 6 it is shown that **1** displaces [³H]CP55,940 in a concentration-dependent manner over two concentration phases. In a first phase (at 10−80 nM), in which only monomers of **1** are present, [³H]-CP55,940 is significantly displaced from the CB$_2$ receptor by
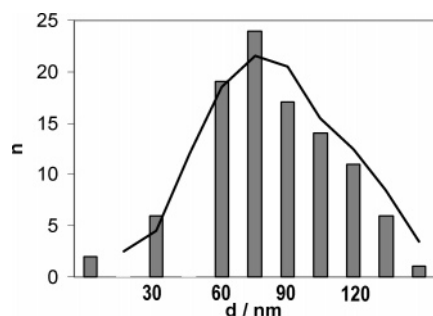
Figure 4. Size distribution of micelles (center to center distance) formed by compound **1** at 200 nM in deionized water at room temperature as measured by dynamic light scattering immediately after incubation. The dark line shows the trend of a moving average. $N = 3$.
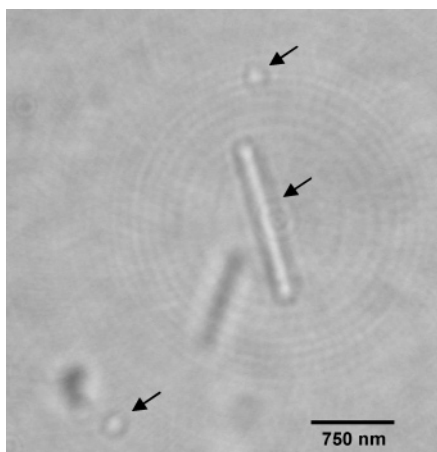
Figure 5. Image of rod-like and globular supermicelles (arrows) formed by compound **1** at 50 μM in deionized water at room temperature after 30 min of incubation. The photograph was obtained with oil immersion ($100\times$ magnification) phase contrast microscopy and was digitally amplified (10-fold).

approximately 50%. When **1** starts to form premicellar aggregates (at 90−140 nM) (see Figure 3), the overall displacement diminishes, and at concentrations at which **1** reaches the CMC (at 200−300 nM) almost no displacement occurs, most likely due to partitioning of the molecules into stable micelles (see Figure 3). At concentrations higher than the CMC (at 600−5000 nM) the micelles aggregate into unstable supermicelles, which are likely to partially dissociate during rearrangement, leading to numerous free monomers, which compete with [³H]CP55,940 for CB₂ receptor binding. That the supermicelles of **1** tend to be colloidally unstable is indicated by the fact that they flocculate over time (*vide supra*). Compound **2** showed a similar first displacement and a subsequent decrease in binding activity (100−1000 nM), which would be a consequence of premicelle formation, but no statistically significant second displacement phase.[4] These findings are in line with the much higher CMC of **2**. In addition, micelles formed by **2** are less compact (*vide infra*) and thus potentially less stable.

In order to develop an understanding of the experimental data on *N*-alkyl amides at a mechanistic level, we have simulated the aggregation process by a stochastic global-energy optimization method (see Experimental Section). The use of $T = 1000$ K helped to make enthalpy the major thermodynamic factor influencing the final Gibbs free energy difference, ΔG. This was important in order to simplify the calculations. First, the ΔG for the aggregation of **1**, **2**, and **3** into dimers and trimers was calculated and compared after extensive global-energy optimization,[13,14] by subtracting the energy of the single free monomers from the energy of the complex. All three molecules aggregated in dimers and trimers with a favorable energy proportional to the number of monomers (Figure 7). The

obtained final ΔG with its van der Waals (vw), electrostatic (el), and surface (sf) energy terms for the trimers made of monomers **1**, **2**, and **3** was respectively −20.91 (vw −34.11, el +2.77, sf −8.2), −33.09 (vw −25.12, el +1.55, sf −8.45), and −22.15 (vw −24.52, el +1.87, sf −8.67). An analysis of the three-dimensional packing of the trimer reveals that **1** and **2** but not **3** have the appropriate shape (hydrophilic heads and hydrophobic tails packed together) to form higher order aggregates (Figure 7). At the monomer level, the hydrophobic chain of **3** exhibits a particular angulation due to the triple bond, which diminishes the water-accessible apolar surface (ASA). On the basis of studies with phospholipids it has been shown that the ASA controls the energetic cost of self-assembly.[15] During the formation of the trimer (Figure 7), to avoid the increase in the enthalpy term ΔH, which would have a disturbing effect on the total ΔG, compound **3** aggregates in a way that keeps the hydrophobic chains distant from each other and without any ordered directionality (as shown by the arrows in Figure 8). While entropy (whose effect is incorporated in a continuous solvent approximation) is likely to also play a role, only enthalpy was calculated, as it is more easily computable. Although it is generally accepted that an aqueous environment is a prerequisite for self-assembly of amphiphilic molecules, hydrophobic interactions are considered to be the major driving force during aggregation.[16] The water-exposed headgroup regions were proved by Heerklotz and Epand to almost not contribute to the ΔG during micelle formation and to be only part of the endothermic interaction enthalpy ΔH_{end}.[15] Thus, the directionality of the hydrophobic chains are of paramount importance for micelle formation.

The aggregation of **1**, **2**, and **3** to a maximum of 16 monomers was followed during Monte Carlo simulations (see Experimental Section). The results obtained for **1**, **2**, and **3** were clearly different from each other. The aggregation of **3** was stopped at the 8 monomer level because, as mentioned before, **3** is not able to align well the hydrophobic side chains during the simulations, indicating that for this molecule self-association is too energetically demanding. This is in agreement with our experimental finding that compound **3** does not form micelles. The attention was then focused on MC simulations of the aggregation with complexes of **1** and **2** of 8 and 16 monomers. At the level of 16 monomers, both molecules aggregate well in the amphiphilic fashion (Figure 8), but **1** has a favorable total Gibbs free energy difference, ΔG (−214.4 kcal/mol for **1** against −179.8 kcal/mol for **2**). Analyzing the difference in the energetic terms between the aggregate and the sum of the monomer-free state, the value of ΔG_{vw} (van der Waals energy term) is similar for **1** and **2**. The ΔG_{to} (torsion energy term) and ΔG_{sf} (surface energy term), instead, are respectively larger (34.74 kcal/mol for **2** against 13.5 kcal/mol for **1**) and smaller for **2** (−64.18 kcal/mol for **2** against −73.54 kcal/mol for **1**). Both aggregates have comparable solvent accessible area, but the 16-monomer complex of **1**, to be able to assemble well by destroying hydrophobic hydration shells and increasing hydrophobic contacts with favorable van der Waals interactions, pays the penalty of having more torsion angles out of range.

Thus, the 16-monomer complex of **1** during simulations is more compact thanks to a better alignment of the hydrophobic chains, and hence, the monomer **1** is a better aggregator. Another feature that might influence the CMC is the geometrical curvature of the aggregate of **1**. When the aggregates of **1** and **2** after simulations are compared (Figure 8), it is evident that the curvature of monomer **1** is much higher than **2**, which indicates that **1** requires a smaller number of monomers to form micelles. By approximating the atomic density of the two aggregates (Figure 8) to an ellipsoid, it is possible to calculate the values of the half-axis of the ellipsoid, which are (9.21 nm, 6.35 nm, 4.84 nm) and (7.05 nm, 6.7 nm, 6.2 nm) for **1** and **2**, respectively. This reveals again that **1** is an ideal aggregator, which is also confirmed by its exceptionally low CMC (200−300 nM) determined experimentally.
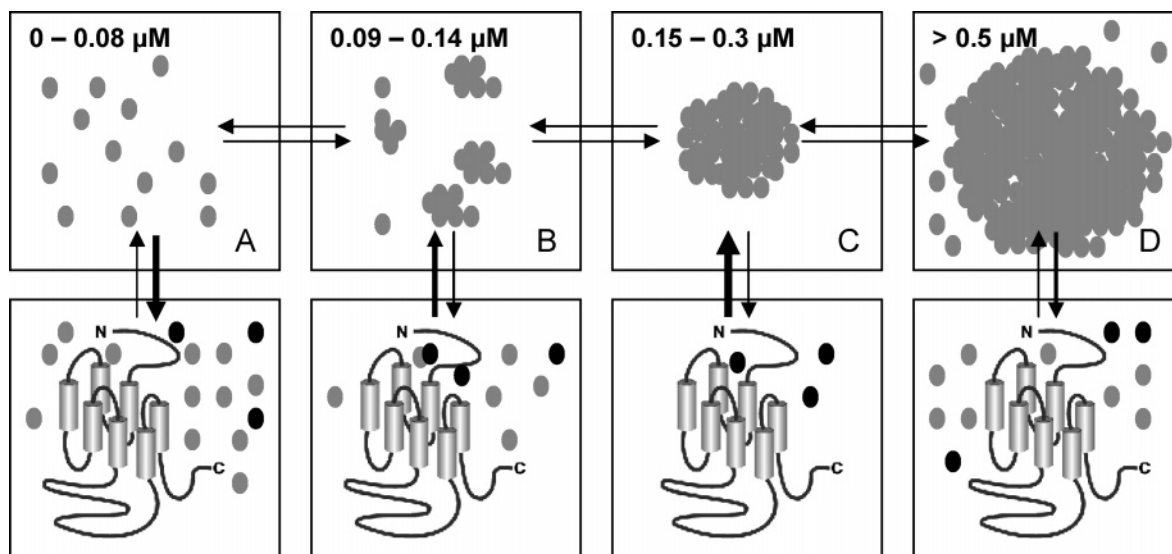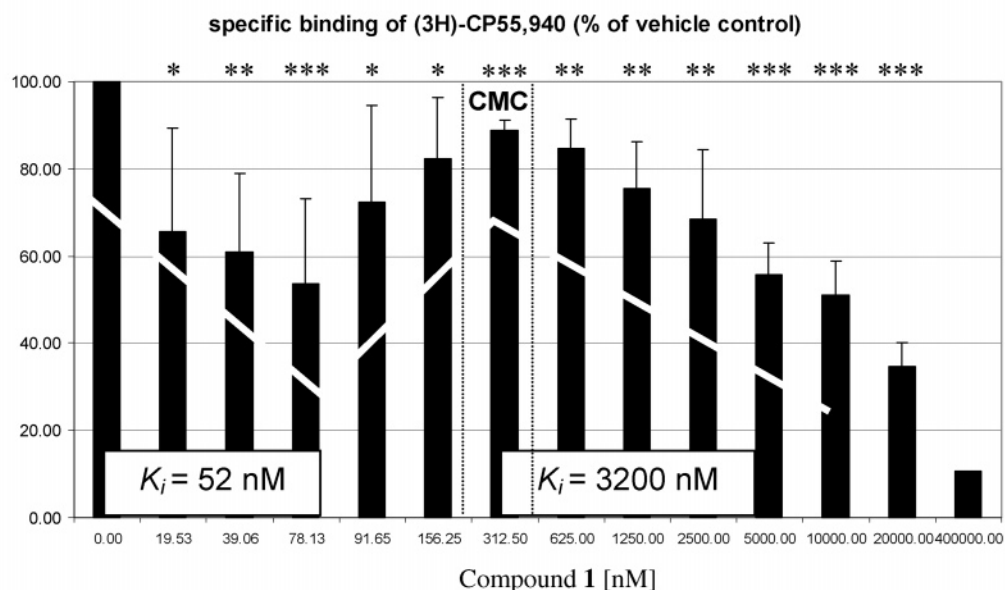
Figure 6. (a) Partition model of *N*-alkyl amide **1** aggregation states (A, monomers; B, premicelles; C, micelles; D, supermicelles) between water, an aggregation phase, and the CB$_2$ receptor. Gray spheres indicate *N*-alkyl amide **1** molecules, and black spheres the CB$_2$ receptor radioligand [^{3}H]CP55,940. (b) Experimental data of increasing concentrations of **1** on [^{3}H]CP55,940 displacement from CB$_2$ showing a biphasic curve (white line) with two possible K_i values. $N = 4 \pm$ SD. *$p = \leq 0.05$; **$p = \leq 0.01$; ***$p = \leq 0.001$.

Concluding Remarks

Fatty *N*-alkyl amides from the medicinal plants *Echinacea purpurea* and *Echinacea angustifolia* have recently regained attention as pharmacologically interesting compounds, particularly because of their described affinity to cannabinoid receptors.[4] Since the outcome of both *in vitro* and *in vivo* experiments depends on the solubility and conformation of test compounds, it is important to understand their physicochemical behavior in an aqueous environment. While the endogenous cannabinoids anandamide and 2-AG do not aggregate and thus freely interact with the CB$_2$ receptor, **1** partitions between the CB$_2$ receptor-bound, the free monomer, premicellar, and micellar states and therefore exhibits differential CB$_2$ receptor affinity as a function of concentration. Thus, at the concentration (CMC) at which **1** assembles into micelles, the molecules aggregate and no longer bind to the CB$_2$ receptor. To the best of our knowledge, the CMC range for **1** is the lowest reported for a bioactive natural product. These findings have implications for pharmacological studies with this class of compounds and imply that *N*-alkyl amides should be assessed for their aggregating behavior prior to performing biological assays. Moreover, the self-assembly of **1** and **2** into micelles, which are stable at concentrations close to the CMC, may serve as a carrier and drug delivery system for poorly soluble compounds in plant extracts.

Experimental Section

General Experimental Procedures. Compounds were checked for identity and integrity by thin-layer chromatography and ^{1}H NMR (500 MHz, Bruker) spectroscopy prior to use. Fluorescence measurements were performed on a GeniosPro plate reader (Tecan, Switzerland). Aggregates were analyzed on a 3000HS Zetasizer (Malvern Instruments Ltd.) equipped with a He−Ne ion laser (633 nm).

Sample Preparation. Dodeca-2*E*,4*E*-dienoic acid isobutylamide (**1**) was isolated from *E. purpurea* as previously published[5] from *Echinacea* root material. Dodeca-2*E*,4*E*,8*Z*,10*Z*-tetraenoic acid isobutylamide (**2**) and undeca-2*E*-ene-8,10-diynoic acid isobutylamide (**3**) were obtained as a gift from Prof. Dr. R. Lehmann (MediHerb, Australia). Anandamide

		Compound		
		1	**2**	**3**
Aggregation level	dimer (kcal/mol)	- 10.94	- 14.90	- 11.11
	trimer (kcal/mol)	- 20.91	- 33.09	- 22.15
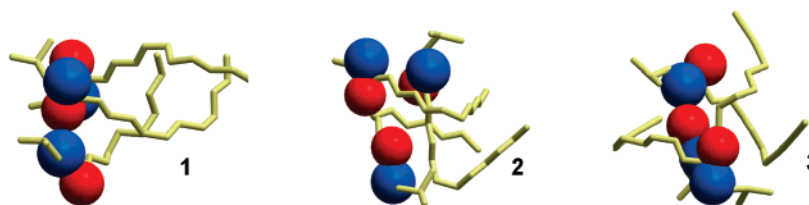
Figure 7. Gibbs energy value (kcal/mol) for dimer (first-row) and trimer (second-row) aggregates. Trimer aggregates of **1**, **2**, and **3** after Monte Carlo simulation are shown with the carbon atoms of the hydrophobic chain colored in yellow and displayed as sticks and with the nitrogen and oxygen atoms colored in blue and red, respectively, and displayed as cpk (ICM v3.4-2b).
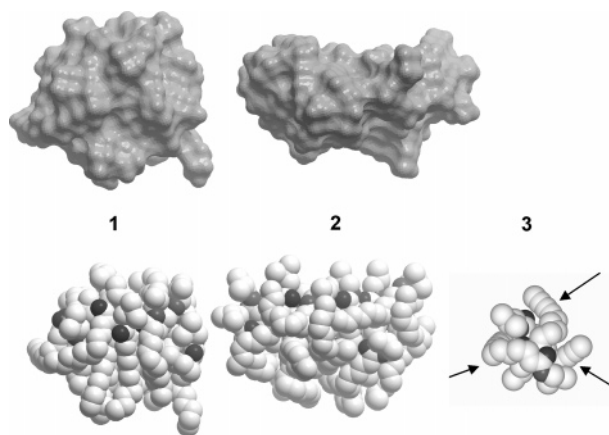
Figure 8. The 16-monomer aggregates of **1** and **2** after Monte Carlo simulation. A trimer aggregate of **3** after Monte Carlo simulation is shown with carbon atoms of the hydrophobic chain indicated by arrows. Atoms are displayed as Connolly surface and cpk (ICM v3.4-2b).

and 2-AG were obtained from Tocris Cookson Ltd (UK). Compounds were dissolved in DMSO (2 mM stock solutions). Nanopure distilled water was used for the preparation of buffers. Samples were filtered through quantitative Millipore filters (Grade 221).

Determination of Tyndall Effect. Colloidal suspensions obtained at RT were added to a glass cuvette and irradiated with a 645 nm, class IIIA red laser (output power 4.2 mW). Tyndall effect positive suspensions showed the laser beam traveling through the medium. The Tyndall effect increases to the third power of particle size for any given concentration.

Phase Contrast Microscopy. Colloidal suspensions were added to a glass slide and immediately analyzed on a phase contrast Aristoplan microscope (Leica Instruments, Heidelberg) using a $100\times/1.4.$ -. 0.7 oil immersion objective. Images were recorded on a digital camera (Nikon Coolpix 4500) and digitally amplified.

Photon Correlation Spectroscopy. This method is also referred to as dynamic light scattering and quasi-elastic light scattering. It is applicable to particles suspended in a liquid, which are in a state of random movement due to Brownian motion (i.e., particles generally of $2-3$ μm diameter and smaller). The pace of the movement is inversely proportional to particle size (the smaller the particles are, the faster they move, or diffuse), and the pace can be detected by analyzing the time dependency of the light intensity fluctuations scattered from the particles when they are illuminated with a laser beam. A major complication of light scattering studies is dust particles in the sample. Therefore, careful filtering procedures have been applied. Hydrodynamic diameters (d_H, nm) were calculated from the diffusion coefficient (D) using the Stokes−Einstein equation: $d_H = kT/3\pi\eta D$, where k is the Boltzmann constant, T the absolute temperature, and η the viscosity of the solvent. Size distribution was measured at an angle of 90° at RT with the CONTIN method.[11] Samples that yielded a polydispersity index of <0.7 were considered to be sufficiently homogeneous for analysis. Particle size distributions were calculated by transforming the intensity−intensity correlation functions with the CONTIN 2DP algorithm. CONTIN is a generic model that allows fitting of multimodal distributions.

Fluorescence Spectroscopy. Dye micellization was carried out with a modified version of the method described by Eliyahu et al.[10] Compounds (from 2 mM stock solutions) were incubated at increasing concentrations with 0.1 nM fluorescein (free acid, 99%, Fluka, Switzerland) for 90 min at 30 °C in Nanopure distilled water. Experiments were carried out on 96-well microtiter plates (excitation at 485 nm, emission at 535 nm). Since the emission of fluorescein is pH-dependent, the pH of the mixture was kept constant at 6.9. The CMC range was determined as the concentration range where the first statistically significant increase in fluorescence was detected. At an appropriate resolution of the concentration range this increase was not gradual but sudden.

Radioligand Displacement Assays on CB_2 Receptors. Binding experiments were performed in the presence of 0.11 nM of the radioligand [³H]CP-55,940 at 30 °C in siliconized glass vials together with 3.8 μg of membrane recombinantly overexpressing CB_2 (RBXCB2M; Perkin-Elmer Life Sciences), which was resuspended in 0.6 mL (final volume) of binding buffer (50 mM Tris-HCl, 2.5 mM EGTA, 5 mM $MgCl_2$, 0.5 mg/mL fatty acid free bovine serum albumin, pH 7.4). Test compounds were present at varying concentrations, and the nonspecific binding of the radioligand was determined in the presence of 10 μM CP-55,940. After 90 min of incubation, the suspension was rapidly filtered through 0.05% polyethylenimine presoaked GF/C glass fiber filters on a 96-well cell harvester and washed nine times with 0.5 mL of ice-cold washing buffer (50 mM Tris-HCl, 2.5 mM EGTA, 5 mM $MgCl_2$, 2% bovine serum albumin, pH 7.4). Radioactivity on filters was measured with a Beckman LS 6500 scintillation counter in 3 mL of Ultima Gold scintillation liquid. Data collected from four independent experiments performed in triplicate were normalized between 100% and 0% specific binding for [³H]CP-55,940. These data were graphically linearized by projecting Hill plots, which allowed the calculation of IC_{50} values. Derived from the dissociation constant (K_D) of [³H]CP-55,940, the concentration-dependent displacement (IC_{50} value), radioligand concentration (L), and the inhibition constants (K_i) of competitor compounds were calculated using the Cheng−Prusoff equation ($K_i = IC_{50}/(1 + L/K_D)$).[17]

Molecular Mechanics by Monte Carlo Simulation. The molecular system is described in the internal coordinate space using the extended ECEPP/3 force field,[14,18] including van der Waals, electrostatic, hydrogen bonding, and torsion energy terms in aqueous environment. The solvation electrostatic energy term accounting for the water−solute interactions was added to the *in vacuo* energy using efficient implementation of the generalized Born algorithm.[13] The surface energy term for hydrophobic interactions is based on atomic solvent-accessible surfaces. The surface tension is evaluated as a product of the total solvent accessible area by the surface tension parameter of 0.012 kcal/mol/A². The surface tension term is evaluated at each global optimiza-

tion step. The stochastic global-energy optimization method consists of (i) random conformational change of free positional and torsion variables according to the biased probability Monte Carlo (BPMC) method;[13] (ii) local energy minimization of analytically differentiable terms, followed by total energy re-evaluation including the solvation energy; and (iii) acceptance or rejection on the basis of Metropolis criterion[19] applied to the total energy. The temperature of the simulations was set to $T = 1000$ K. The water and solute dielectric constant (ϵ) were set to 78.5 and 4.0, respectively.

References and Notes

(1) Goel, V.; Lovlin, R.; Barton, R.; Lyon, M. R.; Bauer, R.; Lee, T. D.; Basu, T. K. *J. Clin. Pharmacol. Ther.* **2004**, *29*, 75−83.

(2) Barnes, J.; Anderson, L. A.; Gibbons, S.; Phillipson, J. D. *J. Pharm. Pharmacol.* **2005**, *57*, 929−954.

(3) Hall, M.; Nazir, N. *Altern. Ther.* **2005**, *11*, 34−37.

(4) Raduner, S.; Majewska, A.; Chen, J. Z.; Xie, X. Q.; Hamon, J.; Faller, B.; Altmann, K.-H.; Gertsch, J. *J. Biol. Chem.* **2006**, *281*, 14192−14206.

(5) Gertsch, J.; Schoop, R.; Kuenzle, U.; Suter, A. *FEBS Lett.* **2004**, *577*, 563−569.

(6) Chen, Y.; Fu, T.; Tao, T.; Yang, J.; Chang, Y.; Wang, M.; Kim, L.; Qu, L.; Cassady, J.; Scalzo, R.; Wang, X. *J. Nat. Prod.* **2005**, *68*, 773−776.

(7) Klein, T. W. *Nat. Rev. Immunol.* **2005**, *5*, 400−411.

(8) Torchilin, V. P. *J. Controlled Release* **2001**, *73*, 137−172.

(9) Pusey, P. N. In *Liquids, Freezing and the Glass Transition*; Levesque, D., Hansen, J. P., Zinn-Justin, J., Eds.; Les Houches, Session LI, North-Holland: Amsterdam, 1991.

(10) Eliyahu, M.; Makovitzki, A.; Azzam, T.; Zlotkin, A.; Joseph, A.; Gazit, D.; Barenholz, Y.; Domb, A. J. *Gene. Ther.* **2005**, *12*, 494−503.

(11) Ruf, H. *Biophys. J.* **1989**, *56*, 67−78.

(12) Cuesta, J. A.; Sear, R. P. *Eur. Phys. J.* **1999**, *8*, 233−243.

(13) Totrov, M. *J. Comput. Chem.* **2004**, *25*, 609−619.

(14) Abagyan, R.; Totrov, M. *J. Mol. Biol.* **1994**, *235*, 983−1002.

(15) Heerklotz, H.; Epand, R. M. *Biophys. J.* **2001**, *80*, 271−279.

(16) Blokzijl, W.; Engberts, J. B. F. N. *Angew. Chem., Int. Ed. Engl.* **1993**, *32*, 1545−1579.

(17) Cheng, Y. C.; Prussoff, W. H. *Biochem. Pharmacol.* **1973**, *22*, 3099−3108.

(18) Momany, F. A.; McGuire, R. F.; Burgees, A. W.; Scheraga, H. A. *J. Phys. Chem.* **1975**, *79*, 2361−2381.

(19) Metropolis, N. A.; Rosenbluth, A. W.; Rosenbluth, N. M.; Teller, A. H.; Teller, E. *J. Chem. Phys.* **1953**, *21*, 1087−1092.